© 2014. Published by The Company of Biologists Ltd | The Journal of Experimental Biology (2014) 217, 1588-1600 doi:10.1242/jeb.082271

RESEARCH ARTICLE

Aperture effects in squid jet propulsion

Danna J. Staaf*, William F. Gilly and Mark W. Denny

ABSTRACT

Squid are the largest jet propellers in nature as adults, but as paralarvae they are some of the smallest, faced with the inherent inefficiency of jet propulsion at a low Reynolds number. In this study we describe the behavior and kinematics of locomotion in 1 mm paralarvae of *Dosidicus gigas*, the smallest squid yet studied. They swim with hop-and-sink behavior and can engage in fast jets by reducing the size of the mantle aperture during the contraction phase of a jetting cycle. We go on to explore the general effects of a variable mantle and funnel aperture in a theoretical model of jet propulsion scaled from the smallest (1 mm mantle length) to the largest (3 m) squid. Aperture reduction during mantle contraction increases propulsive efficiency at all squid sizes, although 1 mm squid still suffer from low efficiency (20%) because of a limited speed of contraction. Efficiency increases to a peak of 40% for 1 cm squid, then slowly declines. Squid larger than 6 cm must either reduce contraction speed or increase aperture size to maintain stress within maximal muscle tolerance. Ecological pressure to maintain maximum velocity may lead them to increase aperture size, which reduces efficiency. This effect might be ameliorated by nonaxial flow during the refill phase of the cycle. Our model's predictions highlight areas for future empirical work, and emphasize the existence of complex behavioral options for maximizing efficiency at both very small and large sizes.

KEY WORDS: Jet propulsion, Squid, Scaling, Efficiency, *Dosidicus gigas*

INTRODUCTION

Marine larvae tend to propel themselves either with ciliary action or muscular flexion of the body or fins. Jet-propelled squid paralarvae are a striking exception. Jet propulsion in paralarvae, as in adult squid, is accomplished with contractions of circular muscle fibers of the mantle. Water is expelled from the mantle through a muscular funnel that can be aimed to direct the jet and therefore the direction of swimming. Owing to the energetic loss of accelerating a relatively small jet of water to high speed, as well as the costly refilling period, during which there is no active thrust, squid jet propulsion is inherently inefficient in comparison to undulatory locomotion in fish (O'Dor and Webber, 1986; O'Dor and Webber, 1991). Efficiency of jet propulsion in squid can be improved by climb-and-glide jetting (Gilly et al., 2012), but this option is also open to fish (Schaefer et al., 2007), leaving squid still at a disadvantage. However, one possible efficiency-increasing measure is unique to pulsed jet locomotion: the formation of vortex rings. These have been shown to increase the swimming efficiency of paralarval *Doryteuthis pealeii* (Bartol et al., 2009a) and juvenile and adult *Lolliguncula brevis* (Bartol et al., 2009b).

Hopkins Marine Station of Stanford University, Oceanview Boulevard, Pacific Grove, CA, 93950, USA.

*Author for correspondence (dannajoy@gmail.com)

Received 26 October 2012; Accepted 10 January 2014

Adult squid can also supplement jet propulsion with undulatory activity of the fins, but during fast escape jets, which are crucial to a squid's survival, the fins are wrapped around the body and do not contribute to propulsion (O'Dor, 1988a). As for paralarvae, their relatively tiny fins provide little thrust (Hoar et al., 1994). These small jet propellers also face the challenges of operating at low Reynolds numbers, where viscous forces dominate over inertia. At Reynolds numbers above ~1000, inertia from the contraction phase can continue to carry the squid forward during the refill phase, providing the energetic advantage of a burst-and-coast swimming technique. But in the low Reynolds number regime, this method is nearly impossible (Weihs, 1974).

These and other factors have stimulated studies on the mechanics of paralarval jet propulsion, but work has been limited to a few species. Escape responses, the fastest jets of squid, have been analyzed in embryonic and hatchling *Doryteuthis opalescens* of 2–3 mm mantle length (ML) (Gilly et al., 1991) and in hatchling *Sepioteuthis lessoniana* of 5–7 mm ML (Thompson and Kier, 2001; Thompson and Kier, 2006). A variety of jetting styles have been studied in paralarvae of *D. pealeii* (1.8 mm ML) (Bartol et al., 2009a).

All three of the above species, along with most other squid selected for study of swimming kinematics (e.g. Anderson and DeMont, 2000; Anderson and Grosenbaugh, 2005; Thompson and Kier, 2001), belong to the family Loliginidae, as these nearshore species are generally the easiest to maintain and breed in culture. Locomotion in oceanic squid remains largely unstudied, and there is reason to believe it is quite different from nearshore squid locomotion. Members of one oceanic family, Ommastrephidae, typically hatch at half the length of loliginids and an earlier stage of development, but immediately begin active swimming behavior (O'Dor et al., 1986; Staaf et al., 2008), the mechanics of which have never been studied.

At less than a millimeter in mantle length, ommastrephid hatchlings may be the smallest squid in existence, but adults of these same species can exceed 1 m ML. In general, squid face a range of Reynolds numbers from ~1 as paralarvae to ~10^8 as the largest adults (Bartol et al., 2008). How can the same swimming mechanism be used at all sizes?

Several features relevant to jet propulsion scale with body size in squid and serve to guide our attempt to answer this question. The overall shape of the mantle changes during ontogeny, such that paralarvae are relatively shorter and wider than adults. This may aid stabilization while fins are too small to perform this role (Hoar et al., 1994). Paralarvae also exhibit more frequent mantle contractions than adults, enabling them to maintain forward momentum despite their inability to glide (Thompson and Kier, 2001; Preuss et al., 1997). Finally, the area of the funnel aperture relative to body size is larger in paralarvae than in adults.

Because the muscular funnel is under the squid's control, the size of the funnel aperture is of particular interest in regard to the scaling of jet propulsion with body size. Unfortunately, its contribution to locomotion is difficult to quantify and consequently has been largely

The Journal of Experimental Biology

The Journal of Experimental Biology (2014) doi:10.1242/jeb.082271

List of symbols and abbreviations

A	aperture area
B_g	frontal body area during sinking
B_s	frontal body area during upward swimming
C_d	coefficient of drag
CMP	central mitochondria-poor fibers
d	coefficient of discharge
F_d	drag
L	mantle length (in equations)
M_{eff}	effective mass
ML	mantle length
MW	mantle width
n	coefficient of nonaxial flow
P	total mantle-cavity pressure
P_j	jet pressure
P_T	pressure from thrust
P_μ	pressure from viscous effects
r_a	aperture radius
Re	Reynolds number
r_i	inner mantle radius
r_o	outer mantle radius
S	squid velocity relative to stationary water
SMR	superficial mitochondria-rich fibers
T	thrust
u_g	sinking velocity
u_j	jet velocity relative to squid
u_s	upward swimming velocity
V_i	mantle cavity volume
V_o	squid volume, including mantle cavity
w	mantle thickness
w_r	resting mantle thickness
η	hydrodynamic efficiency
μ	seawater dynamic viscosity
ρ_s	squid tissue density
ρ_w	seawater density
σ	stress

ignored (O'Dor and Webber, 1991). A few empirical studies, however, hint at the importance of funnel control in jet propulsion. At high speeds, an adult *Illex illecebrosus* (Ommastrephidae) increases speed by increasing mantle cavity pressure, which may in turn be caused by restricting the funnel aperture through muscular contraction (Webber and O'Dor, 1986). Control of the funnel aperture has also been observed or suggested in adults of *D. opalescens* (O'Dor, 1988a), *D. pealeii* (Anderson and DeMont, 2000) and *L. brevis* (Bartol et al., 2001). However, this feature has never been incorporated into a theoretical framework of squid jet propulsion.

We present empirical results on the swimming behavior and mechanics of paralarval Humboldt squid, *Dosidicus gigas* (d'Orbigny 1835) (Ommastrephidae), and describe a novel mechanism for restricting the flow between mantle and head, which functionally affects jetting in the same way as active control of the funnel aperture. We then assess the implications of aperture control for propulsive efficiency through a theoretical model that can be scaled over three orders of magnitude, from the tiniest hatchling to a large, powerful adult.

RESULTS

Behavior

Paralarvae demonstrated a variety of swimming behaviors, most of which fell into one of three clear categories: maintenance jetting, slow jetting and fast single jets. If not actively swimming, paralarvae always sank, at a rate of −0.46±0.02 cm s^{-1} (N=3). Maintenance jetting consisted of individual jets that just counteracted this rate, thereby maintaining the vertical position of the paralarva in the water column. During this behavior, the distance the animal moved up during each jetting period was roughly equal to the distance it moved down during each refilling period, and net velocity was approximately zero. Jetting frequency during maintenance jetting was 2.13±0.44 Hz (N=3).

Slow jetting consisted of prolonged periods of repeated jets, usually vertical, during which the paralarva reached a maximal net velocity of 0.51 cm s^{-1} (~5 ML s^{-1}). Periods of slow jetting thus moved the animal upward, often to the surface. These periods were usually followed by periods of sinking that lasted much longer than a single refilling period and during which no active swimming was observed. This combination of slow swimming and sinking resembled the hop-and-sink behavior described for other negatively buoyant zooplankton (Haury and Weihs, 1976).

Fast single jets were individual jets that launched the animal out of the field of view, and appeared to be similar to the escape jets of adult squid. The maximal speed measured in one of these jets was 2.34 cm s^{-1} (~23 ML s^{-1}).

The dominant swimming direction was vertical, although paralarvae showed the ability to change direction extremely rapidly. Occasionally, they would engage in circular jetting, a period of several fast jets, which departed notably from the standard maintenance or slow jetting. These sequential jets were angled so the squid traced a circular path through the water, as though following a racecourse. The direction of swimming during circular jets was always fins-first, unlike the slower lateral circling in which paralarval *D. opalescens* orient arms-first toward their prey, orbiting it as the moon orbits the earth (Chen et al., 1996). Both circular jetting and fast single jets could represent escape behavior, although they often occurred without any startling stimulus that was obvious to the observer.

Paralarvae also demonstrated a distinctive pulsing behavior with high contraction frequency (4.5±0.84 Hz, N=3); the maximal frequency measured was 5.4 Hz. During these episodes they neither sank nor moved an appreciable distance, and displayed almost no oscillatory up–down motion. Pulsing episodes were observed in all paralarvae and lasted 1–9 s.

Kinematics

Fig. 1 shows representative traces of maintenance jetting (Fig. 1A), slow jetting (Fig. 1B) and a fast single jet (Fig. 1C) taken from standard videos (30 frames s^{-1}). Slow/maintenance jets (Fig. 1D) and fast single jets (Fig. 1E) are also shown from high-speed videos (Fig. 1D,E). It was not possible to distinguish maintenance jetting from slow jetting in high-speed videos, which were recorded after placing paralarvae in 50 mm diameter plastic culture dishes. The shallow depth (~5 mm) of water in the dishes may also have introduced wall effects. For these reasons, we avoided pooling our data, and instead made separate comparisons between jets in a more open environment (recorded with standard videos) and between jets in dishes (recorded with high-speed videos). Although the exact velocities measured under wall-effect conditions may be distorted, measurements of the mantle kinematics used to achieve these velocities should still be informative.

Mantle width, measured at the widest part of the mantle and normalized by dorsal mantle length, is shown in all panels of Fig. 1. Mantle aperture width, also normalized by mantle length, is shown for the high-speed traces. Closure of the mantle aperture proceeds in tandem with mantle contraction, though more rapidly, presumably forcing water to be expelled through the funnel alone, rather than 'leaked' through the mantle opening. Selected high-speed video frames from a single fast jet are shown in Fig. 1F to illustrate closing of the mantle aperture around the head.

The Journal of Experimental Biology (2014) doi:10.1242/jeb.082271

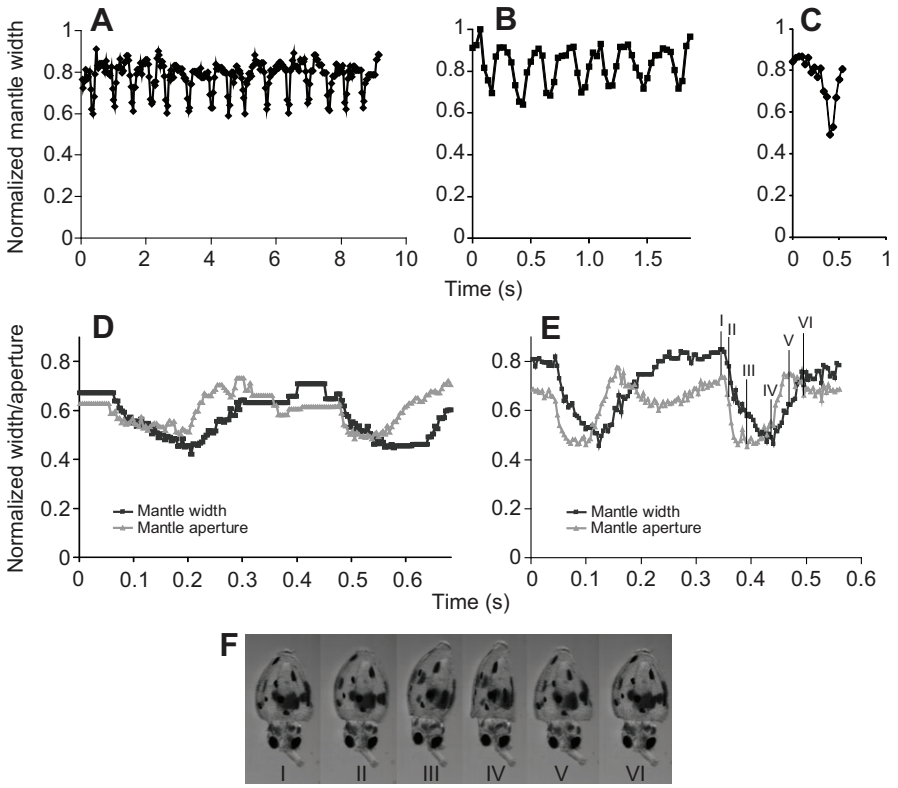

Fig. 1. The different types of jetting of *Dosidicus gigas*. (A–C) Representative traces from standard 30 frames s^{-1} videos of maintenance jetting (A), slow jetting (B) and fast single jets (C). (D,E) Representative traces from high-speed videos of slow jets similar to maintenance jetting or slow jetting (D) and fast single jets (E). Normalized mantle width is shown in all panels; normalized mantle aperture is also shown for the high-speed traces. (F) Video frames of closure of the mantle aperture during a single fast jet (as in E).

When all jets from standard videos were analyzed together, including both slow jetting and fast single jets, the velocity of the squid showed a modest inverse relationship (Fig. 2A, R^2=0.23) with minimal mantle width. Faster jets occurred when the mantle contracted to a smaller diameter (a smaller minimal mantle width), thereby expelling more water.

Standard video sampling of 30 frames s^{-1} was too slow to accurately track the speed of individual contractions, so we assessed the rate of mantle contraction by counting the number of contractions over a longer period of time. It is not possible to assess this statistic for individual jets, so data in Fig. 2B were derived only from slow jetting sequences. The R^2 value of 0.45 suggests that hatchlings may increase the rate of mantle contraction in order to move faster. This is consistent with the observation that jet frequency is the primary mechanistic difference between maintenance jetting and slow jetting.

Using measurements of individual jets made with high-speed video sampling, Fig. 3 shows that contraction time, minimal mantle width, and mantle aperture width are all negatively correlated with squid velocity for single jets. Two clusters of data appear for mantle aperture width (Fig. 3C). This appears to be a binary rather than a continuous variable – either paralarvae allow water to leak out around their heads, behaving more like a jellyfish than a squid, or they clamp the mantle down and expel water only through the funnel. ‘Sealed’ jets are faster.

ANOVA of the generalized linear model (GLM) of squid velocity showed that only aperture width was a significant predictor of velocity (P<0.001). Further statistical analysis confirmed that the most robust GLM of squid velocity uses a single, binary ‘leaky or sealed’ variable. A GLM including contraction time, minimal mantle width and aperture width as a continuous variable had an Akaike information criterion (AIC) of 102, whereas a GLM including time, minimal mantle width, and aperture width as a binary variable had an AIC of 95, and a GLM with only binary aperture width had an AIC of 92 (lower AICs indicate a better fit).

Model

Specific model simulations were run for 1 mm paralarvae to compare with empirical results. A leaky paralarva, with aperture

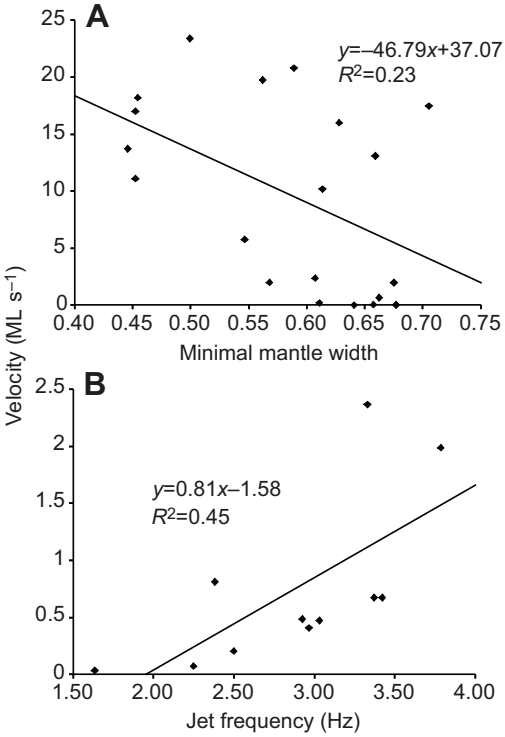

Fig. 2. Kinematics of paralarval *D. gigas* swimming, from standard 30 frames s^{-1} video clips. (A,B) Velocity plotted against the minimal mantle width (A; ratio of fully contracted to fully expanded mantle, smaller numbers indicate more contraction) and frequency of contraction (B); single fast jets were excluded, because frequency cannot be calculated.

The Journal of Experimental Biology (2014) doi:10.1242/jeb.082271

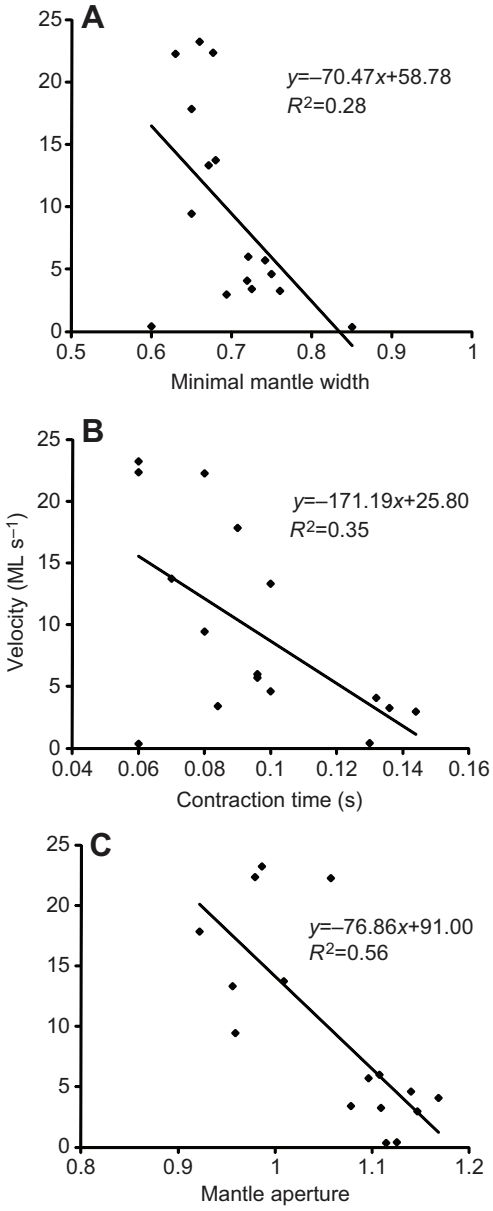

Fig. 3. Kinematics of paralarval *D. gigas* swimming, from high-speed video clips. (A–C) Velocity plotted against minimal mantle width (A), contraction time (B) and aperture closure (C).

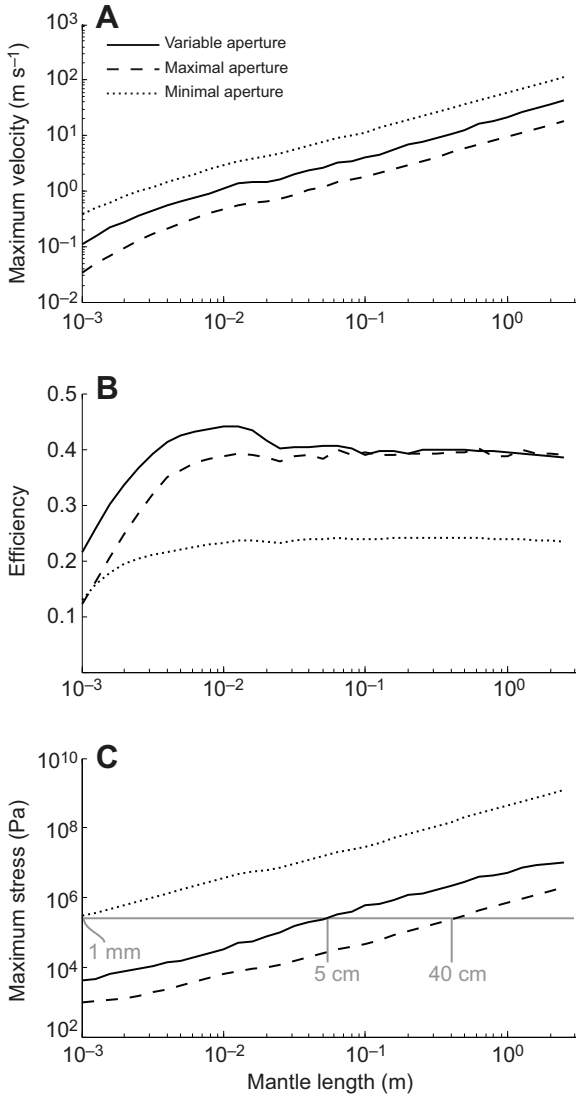

Fig. 4. Size-dependent scaling of squid jet propulsion and the effect of jet aperture area. Theoretical results for (A) maximal squid velocity at the peak of a single jet, (B) hydrodynamic efficiency summed over 10 jet cycles, and (C) maximal stress on the mantle muscle at the peak of a single jet. Models with a constant small aperture area (dotted line), a constant large aperture area (dashed line) and a dynamically varying aperture area (solid line) are shown. A horizontal gray line in C indicates a maximal muscle stress of 2.5×10^5 N m^{-2}. Mantle lengths at which this stress is reached for each of the three models are given in gray.

area constant throughout the jetting cycle, swims with an average velocity of 0.8 cm s^{-1}, an aperture-controlling paralarva with an average velocity of 2.9 cm s^{-1}. These values are somewhat greater than, but comparable with, our empirical measurements of 0.5 cm s^{-1} for slow jetting and 2.3 cm s^{-1} for fast jets. Including the effects of gravity and a variable jetting frequency, we found that a leaky paralarva contracting at about 2 Hz holds its position in the water, neither rising nor sinking. This value is consistent with frequencies measured for empirical maintenance jetting (2.13±0.44 Hz, N=3).

Iterating the model simulation over squid ML from 1 mm to 3 m showed that maximal velocity of the squid and maximal stress in the mantle muscle increase at a fairly constant rate as the squid grows, while efficiency follows a more complex curve (Fig. 4). The inefficiency of jet propulsion at the smallest size is clear, although a paralarva of several millimeters is already as efficient as an adult squid. Efficiency can be increased at small sizes with a variable funnel aperture, although the advantage over a constant large aperture drops off at more than 1 cm and disappears above 10 cm ML. A constant large aperture results in slow swimming and low stress in the mantle, whereas a constant small aperture results in fast swimming and high stress in the mantle. A large aperture greatly improves efficiency at all ML >2 mm. The variable aperture strikes a balance in speed and stress with only minor compromise in the efficiency advantage conferred by a large aperture.

To make these results biologically relevant, we must consider that muscle cannot generate endlessly increasing stress. The maximal isometric tension of striated muscle is 3–5×10^5 Pa (Alexander and Goldspink, 1977). Peak isometric stress in adult *Alloteuthis subulata* is 2.62×10^5 Pa (Milligan et al., 1997). Tension during isotonic contraction, when the muscle is actually shortening, as during mantle

The Journal of Experimental Biology (2014) doi:10.1242/jeb.082271

contraction, must be less than isometric. Gosline and Shadwick have estimated that in squid the muscle tension needed for 100% utilization efficiency of circular mantle muscle is 2×10^5 Pa, and O'Dor suggests that 2.4×10^5 Pa is the most reasonable estimate of maximal stress in these muscles (Gosline and Shadwick, 1983; O'Dor, 1988b).

Peak stress varies for the two different types of fibers, central mitochondria-poor (CMP) and superficial mitochondria-rich (SMR) fibers; in adult *D. pealeii* it is 2.16×10^5 Pa for CMP and 3.35×10^5 Pa for SMR fibers (Thompson et al., 2008). The squid will be limited by the lower value and thus we focused on peak stress in CMP fibers. This appears to be fairly constant across those few squid species that have been measured ($2.16–2.62\times10^5$ Pa), so we used a single value of 2.5×10^5 Pa (solid line in Fig. 4C). Using simple allometric regressions (Stevenson, 1996) to calculate a model squid's jet frequency and mantle aperture from its mantle length, we found that small squid do not achieve the maximal output of mantle muscle, whereas large squid exceed the stress their muscle can withstand. However, Thompson et al. showed that peak stress in the circular muscles of paralarvae is significantly lower than in adults, a point that is addressed in more detail in the discussion (Thompson et al., 2010a).

We therefore altered the model to maintain stress at a constant 2.5×10^5 Pa at all sizes, by adjusting either jet frequency or aperture size. Figs 5 and 6 compare the previously presented model output, in which all parameters vary according to the Stevenson regressions (and aperture area is variable), to this new 'constant stress' model, in which funnel radius (Fig. 5) or jet frequency (Fig. 6) is adjusted. Panel A in each figure indicates the funnel radius or jet frequency at each size that is necessary to produce this stress, and panels B and C show the effects on maximal velocity and efficiency.

A 1 mm squid must either reduce its funnel radius to 0.015 mm (about 20% of the maximal radius predicted by regression) or increase its jet frequency to 50 Hz to satisfy a constant stress of 2.5×10^5 Pa. A 1 m squid must either increase its funnel radius to 2 cm (about twice the maximal radius predicted by regression) or decrease its jet frequency to once every 6 s for the same result. These changes would increase maximal velocity for smaller squid and reduce maximal velocity for larger squid.

In terms of efficiency, if the squid maintains constant stress by changing funnel radius, efficiency is reduced at small and medium sizes, most markedly in the intermediate size range (Fig. 5C). When the squid approaches 50 cm ML, its swimming efficiency matches that of the variable-stress model, and goes on to exceed it at even larger sizes. If, on the other hand, the squid maintains constant stress by varying jet frequency, then 1–2 mm squid can increase their efficiency to more than 30% (Fig. 6C). Once they grow past 3–4 mm, however, their efficiency is equal to that of the variable-stress model.

These results are all based on a coefficient of nonaxial flow of 1; that is, no reduction in thrust due to nonaxial flow during refilling. Varying this coefficient between 1 and 0 reveals that smaller values can significantly improve efficiency (Fig. 7). At all sizes, the effect is most notable for squid maintaining a constant large aperture, and negligible for squid maintaining a constant small aperture. An intermediate effect is seen in squid varying the aperture size. For squid 1 cm and larger, low values of n cause a constant large aperture to be more efficient than a variable aperture, an effect which increases with squid size.

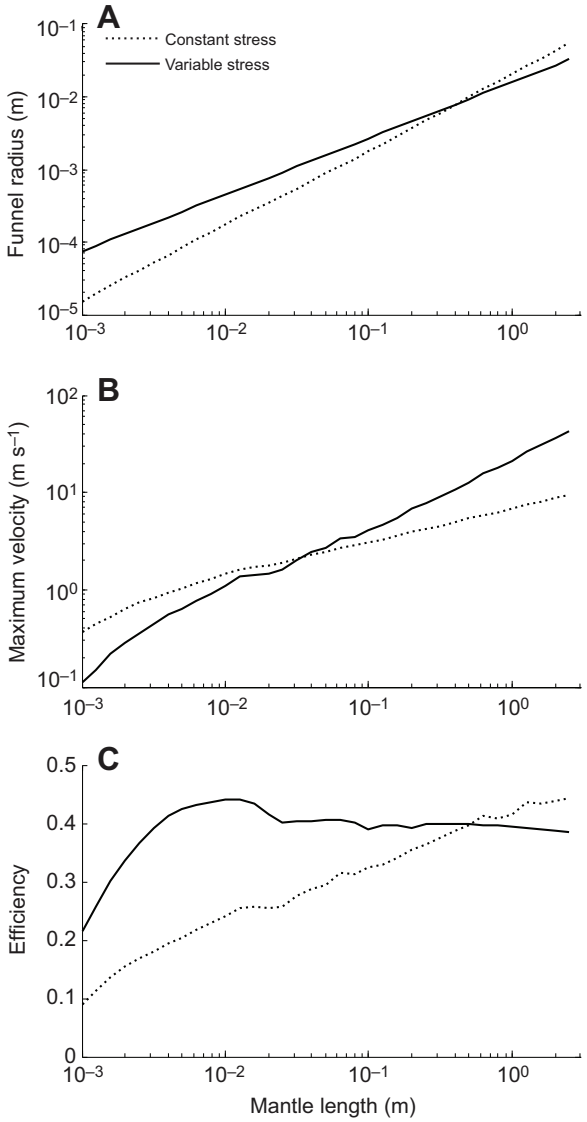

Fig. 5. Size-dependent variation in jetting when variables are set by regressions with a dynamically varying aperture, allowing stress to vary (solid lines), compared with when funnel radius is controlled to maintain a constant stress of 2.5×10^5 N m^{-2} (dotted lines). (A) Size-dependent variation in funnel radius. (B,C) Theoretical results of using this radius for maximal squid velocity at the peak of a single jet (B) and hydrodynamic efficiency (C).

DISCUSSION

Behavior of Humboldt squid paralarvae

Squid swimming has been broken into four distinct categories in adult *D. opalescens* (Hunt et al., 2000): hovering, gliding, slow swimming and jetting. Fins and jet are used together in the first three, whereas only the jet is used in the fourth. *D. gigas* paralarvae exhibit two of these four: hovering (maintenance jetting) and jetting (including slow and fast jetting). The fins of paralarval *D. gigas* are very small and generally erratic in the pattern of flapping, with little obvious effect on whole-animal movement.

Dosidicus gigas paralarvae also exhibit episodes of pulsing, during which the minimal relative mantle width was 0.6–0.7, roughly comparable to what was seen in jetting (Fig. 2). Because pulsing paralarvae did not propel themselves either forward or backward, the water expelled during these contractions must have been largely leaked through the mantle aperture rather than expelled solely through the funnel. Pulsing may be similar to the predatory behavior described by Preuss et al. for hatchling *D. opalescens*, in which attacks on *Artemia* were sometimes prefaced by frequent mantle contractions (exceeding 5 Hz) (Preuss et al., 1997).

The Journal of Experimental Biology (2014) doi:10.1242/jeb.082271

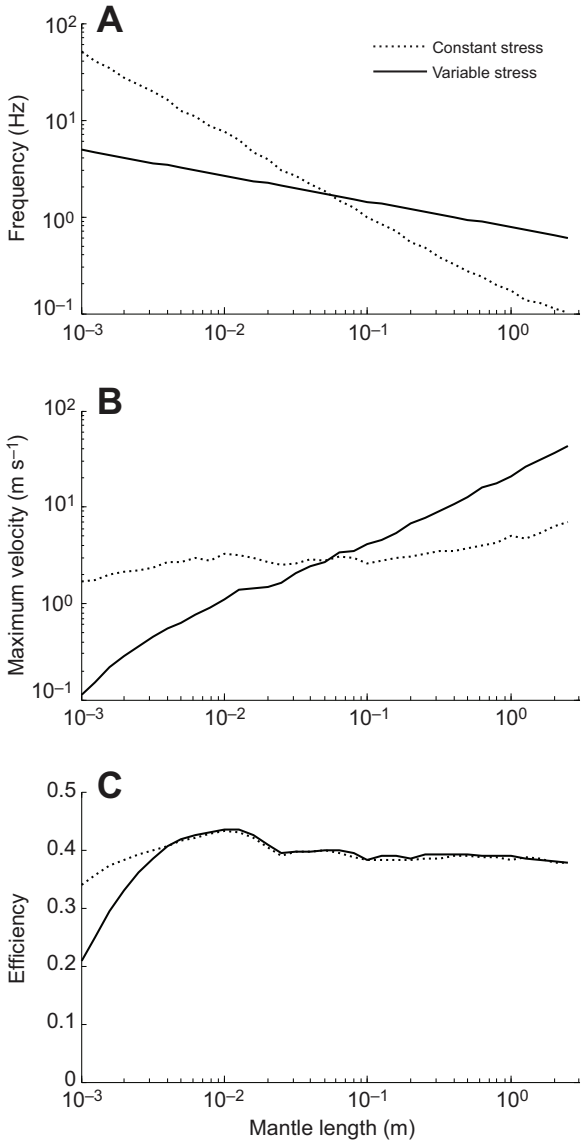

Fig. 6. Size-dependent variation in jetting when variables are set by regressions, and stress is variable (solid lines) compared with when jet frequency is controlled to maintain a constant stress of 2.5×10^5 N m^{-2} (dotted lines). (A) Size-dependent variation in jet frequency. (B,C) Theoretical results of using this jet frequency for maximal squid velocity at the peak of a single jet (B) and hydrodynamic efficiency (C).

Swimming abilities of paralarvae could be used to effect diel vertical migrations, allowing paralarvae to sink to deeper depths during the day to avoid visual predators and rise to the surface at night (Staaf et al., 2008). A vertical climb of 15 m (the depth of the only reported egg mass) by a newly hatched paralarva would take less than 1 h at the observed swimming speed of 0.5 cm s^{-1}, and as the hatchling squid grew, the extent of this diel migration could increase to that of adults (hundreds of meters). Vertical swimming could also facilitate ontogenetic migration, allowing the squid to shift from prime paralarva habitat into prime juvenile habitat. Tens of meters would be sufficient distance to cross a thermocline or sink to a subsurface chlorophyll maximum, which might be a good feeding area, or to rise to the surface, where most paralarvae seem to be caught in plankton nets (Vecchione, 1999; Staaf et al., 2013).

Regular vertical excursions followed by sinking could result in significant energetic savings, as has been demonstrated for numerous negatively buoyant zooplankton (Haury and Weihs, 1976). Hop-and-sink behavior has been reported in other cephalopod paralarvae (Zeidberg, 2004; O'Dor, 1988a; Boletzky, 1974) and may well be an adaptation to save energy, as in the similar strategy of climb-and-glide swimming exhibited by adult *D. gigas* (Gilly et al., 2012).

Considering a vertically oriented animal that seeks to maintain a fixed depth, Haury and Weihs derived an equation for the ratio R of energy required to hop and sink to the energy required to hover (Haury and Weihs, 1976). When R<1, hop and sink is less costly than constant hovering:

$$R = \left[1+\frac{1}{\alpha}\left(\frac{u_s}{u_g}\right)^{2-m}\right]\left[\frac{1}{1+\left(u_s/u_g\right)}\right]\left[1+\frac{u_s}{u_g\alpha^{1/(2-m)}}\right], \quad (1)$$

where u_s is upward swimming velocity, u_g is sinking velocity and:

$$\alpha = \frac{k_g B_g}{k_s B_s}. \quad (2)$$

The constant k depends on the organism's shape during sinking or swimming, and B is the frontal area of the body during sinking or swimming. The variable m in Eqn 1 is a parameter used by Haury and Weihs in their calculation of the coefficient of drag (C_d) as a function of swimming (or sinking) speed. For Renolds numbers (Re) <1, m=1; for Re>1, m approaches zero.

$$C_d = ku^{-m}. \quad (3)$$

Thus, R depends on two factors: the ratio of swimming speed (u_s) to sinking speed (u_g) and the ratio (α) of frontal areas presented in the two modes. The u_s:u_g ratio reported for paralarval ommastrephids is in the range of 1 (Staaf et al., 2008) to 2 (O'Dor et al., 1986). Paralarvae in laboratory observations sink in the direction of the arms, and the arms (sinking) are less streamlined than the mantle tip (swimming upward), so the value of α must be >1. Furthermore, the mantle narrows during swimming. Packard reported that the mantle width of hatchlings (*Loligo vulgaris*) reduced from 2.1 to 1.3 mm during an escape jet, which would correspond to an α of 2.6 (Packard, 1969). According to the predictions of Haury and Weihs (Fig. 2), a speed ratio of 1–2 and an α of 2–3, such as calculated here for *D. gigas* paralarvae, are within the parameter space for energy savings (Haury and Weihs, 1976).

Kinematics of Humboldt squid paralarvae

In studies on the swimming kinematics of *L. brevis*, Bartol et al. found that the smallest size class, 1–2.9 cm ML, increases speed solely by increasing jet frequency, whereas larger squid increase speed by altering mantle contraction to expel greater volumes of water in a given time (Bartol et al., 2001). Very small *D. gigas* paralarvae shift between maintenance and slow jetting, and alter their slow jetting speed, primarily by varying jet frequency, just like small *L. brevis*. Very small *D. gigas* also appear to contract to a slightly smaller minimal mantle width (MW) for faster jetting, unlike small *L. brevis* (Fig. 2) – a difference that may be due to the tenfold difference in size between the smallest studied members of these two species.

In contrast to the frequency-dependent control of maintenance and slow jetting, we found that higher-velocity fast single jets correlated most closely with smaller mantle apertures, and fast jetting thus appears to rely on closing the mantle aperture to increase thrust (Fig. 3). Because of the difficulty of observing very small squid, we do not know whether they are able to control the funnel aperture

The Journal of Experimental Biology (2014) doi:10.1242/jeb.082271

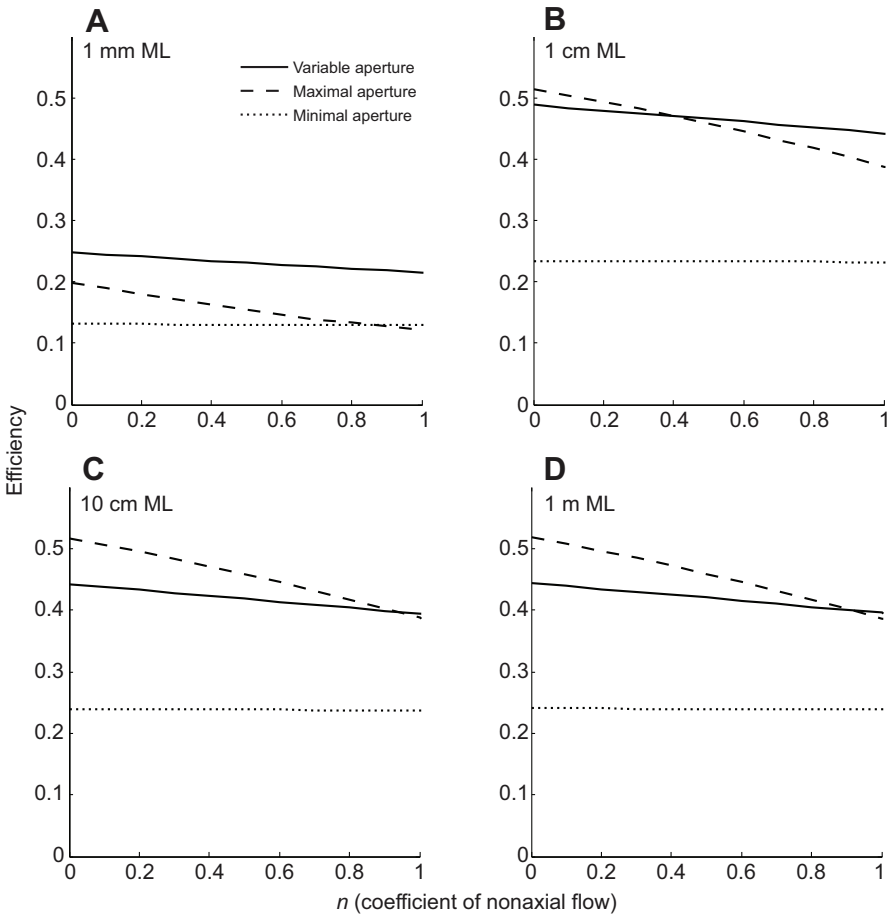

Fig. 7. Effects on whole-cycle hydrodynamic efficiency of *n*, the coefficient of nonaxial flow. Theoretical results for squid of (A) 1 mm ML, (B) 1 cm ML, (C) 10 cm ML and (D) 1 m ML. Models with a constant small aperture area (dotted line), a constant large aperture area (dashed line) and a dynamically varying aperture area (solid line) are shown. This coefficient can also represent pressure effects if permitted to range below 0 and above 1; model runs with values of −0.1 and 1.1 (not shown) were not remarkably different.

itself, but they can clearly alter the total aperture through which water flows by sealing the anterior edge of the mantle around the head (Fig. 1). The much larger area of the mantle aperture compared with that of the funnel suggests that the major increase in thrust derives from closing the mantle aperture.

Fig. 3 suggests that decreasing mantle contraction time and increasing the degree of contraction may assist with increasing jet velocity. Such correlations make intuitive sense. If contraction time decreases, water is expelled in less time, and if the minimal mantle width decreases, a greater volume of water is expelled in a given time. In either case, dV/dt, u_j and thrust would all be increased. These findings contrast with the results of Bartol et al., who found that contraction time increased with increasing velocity, and suggested that an increased contraction time would expel a greater volume of water (Bartol et al., 2009a). These divergent findings may be due to taxonomic or size differences between the study organisms. More data, at a greater range of speeds, from a greater variety of species, would no doubt shed further light on the subject.

One might legitimately ask whether there is any advantage to leaking water through the mantle opening, rather than concentrating all expelled water through the funnel for all jets. O'Dor and Webber point out that, 'Once the mantle becomes an integral part of the jet engine it is impossible to breathe without moving nearly half of the body mass' (O'Dor and Webber, 1991). In the case of *D. gigas* paralarvae, the wide aperture between the head and mantle to some extent uncouples the jet engine from respiration needs. The low-pressure flow through the leaky head-mantle aperture acts more like jellyfish propulsion, allowing the paralarva to remain in place if there is no reason to move, and sealing the mantle around the head leads to high-pressure 'squid-like' propulsion if the paralarva has places to go.

Jet propulsive efficiency throughout ontogeny

Hydrodynamic efficiency of jetting is a matter of considerable biological relevance to squid. More efficient swimming requires less energy, allowing the squid to allocate more resources to growth or reproduction. Because our focus was on the overall ecological importance of efficiency, we chose to consider whole-cycle efficiency, including both contraction and refilling phases of the jet cycle. Thus, our efficiency values are not comparable with those of studies that considered only the propulsive efficiency of the contraction phase (Bartol et al., 2008; Bartol et al., 2009a; Bartol et al., 2009b). Studies that considered whole-cycle efficiency have found values of 38–49% (Anderson and DeMont, 2000; Anderson and Grosenbaugh, 2005) for adult *D. pealeii* (22–30 cm ML) and 29.0–44.6% (Bartol et al., 2001) for juvenile and adult *L. brevis* (1.8–8.9 cm ML). These ranges are similar to our calculated efficiencies for aperture-controlling squid of comparable sizes (Fig. 4B).

The model predicts that 1 mm squid are underperforming, their muscles producing less than maximal stress. In at least one species, the muscles of paralarvae have been shown to have a tolerance of half the 2.5×10^5 Pa value: 1.2×10^5 Pa in *D. pealeii* (Thompson et al., 2010a). However, this is still quite a bit larger than the maximal stress our model predicts for this size of squid. We find that a target value of 1.2×10^5 Pa for a 1 mm paralarva can be achieved by increased jet frequency to 35 Hz or decreasing funnel radius to 0.019 mm. Unfortunately, a frequency of 35 Hz greatly exceeds

The Journal of Experimental Biology (2014) doi:10.1242/jeb.082271

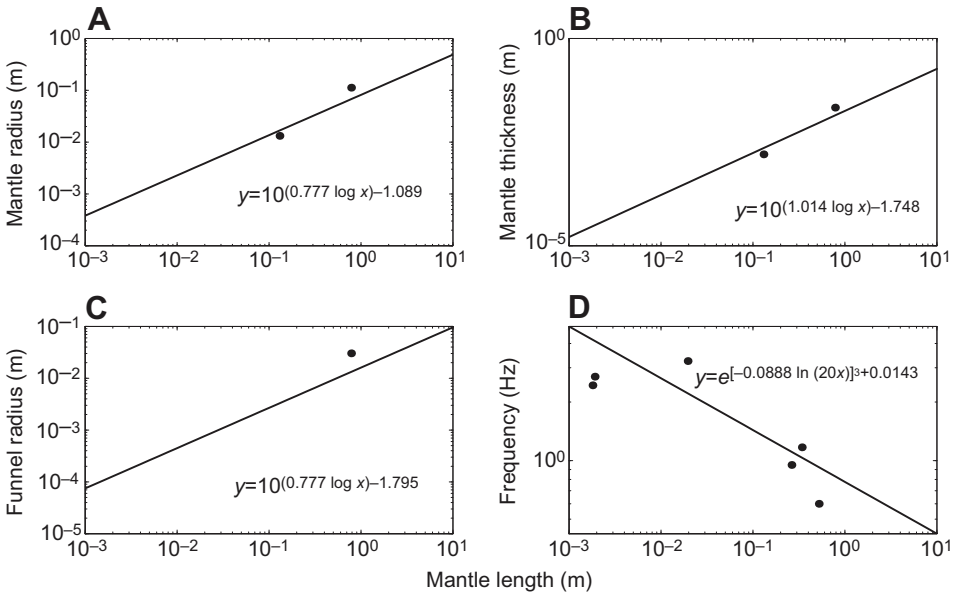

Fig. 8. Allometric growth of squid. Regressions between (A) mantle radius, (B) mantle thickness, (C) funnel radius and (D) jetting frequency and mantle length derived by Stevenson (Stevenson, 1996) based on empirical values (not shown here). Black circles represent additional data points gleaned from the literature (Gosline and Shadwick, 1983; Preuss et al., 1997; Bartol et al., 2009b; Anderson and Grosenbaugh, 2005; O'Dor, 1988b; Bartol et al., 2001) and W.F.G., unpublished data.

biological plausibility (Fig. 6) – indeed, empirical measurements of paralarval frequency are even lower than the modest prediction of ~5 Hz from the equation (Fig. 8) – and decreasing the funnel radius would reduce efficiency to 10% (Fig. 5). Low propulsive efficiency at 1 mm may explain why so many squid hatch in excess of this size. Even squid of 2 mm ML, the size of many loliginid hatchlings, are predicted to be much more efficient. One must wonder how the tiny ommastrephid hatchlings manage. Energy savings from hop-and-sink swimming behavior, as calculated above, may partially answer this question.

Efficiency increases as squid grow to a peak of almost 45% around 1 cm ML (Fig. 4), then begins a slow decline because of ontogenetic decrease in the amplitude of mantle contraction (Thompson and Kier, 2001). Yang et al. observed that juvenile *D. opalescens* develop the ability to hold a stationary swimming position and begin schooling behavior at 1 cm ML (Yang et al., 1986). The ratio of fin to mantle length also increases rapidly in this species at this size. Unpublished data from Hanlon et al. (Hanlon et al., 1979) show an abrupt jump in this ratio from 0.15 in a hatchling of 8 mm ML to 0.23 in a juvenile of 1.7 cm ML, and a further jump to 0.36 in a juvenile of 2.4 cm ML. (The ratio in an adult squid of 9.5 cm ML is 0.47.) A combination of increased hydrodynamic efficiency and relatively larger and more effective fins may be necessary prerequisites for the more complex swimming required to maintain a school. 1 cm ML is also the size at which paralarvae of *D. gigas* transition into juveniles, with the completed separation of their distinctive proboscis into two tentacles (Shea, 2005). This developmental shift has never been observed in live specimens and information is lacking for any accompanying behavioral changes, but the situation could be similar to that of *D. opalescens*.

Once squid reach ~6 cm, they must limit their maximal muscle stress (Fig. 4C). Unlike 1 mm squid seeking to increase muscle stress, these squid have two realistic options: increasing funnel aperture and decreasing jet frequency.

For squid larger than 50 cm ML, increasing funnel aperture not only alleviates stress, it actually increases efficiency. Indeed, the few measured funnel radii of large squid are all larger than the radii predicted for this size range by regression equations (Fig. 8) (see also Stevenson, 1996). The funnel radius of a 78 cm ML adult *D. gigas* was measured by the authors to be 3 cm, comfortably above the 2 cm predicted by the model to limit stress at 2.5×10^5 Pa (Fig. 5A). It is possible that these large squid also control stress by altering their jet frequency; archival tag data from free-swimming adult *D. gigas* (70–80 cm ML) indicate that active jetting during maintained swimming can reach a rate of ~0.1 Hz (Gilly et al., 2012), close to the 0.2 Hz value that places these squid just at the 2.5×10^5 Pa limit (constant stress in Fig. 6A).

For squid between 6 and 50 cm ML, however, an increased funnel aperture reduces efficiency. Reductions in jet frequency offer no such drawback; this would therefore seem to be a preferable solution to the need to reduce muscle stress in the mantle for small and medium squid. But lowering jet frequency results in a greater loss of velocity than increasing aperture size. Thus, even though lowering the frequency saves efficiency, ecological pressures that push for maximal velocity (such as escaping predators) may result in an increased aperture size – and a concurrent drop in efficiency.

Depending on the coefficient of nonaxial flow during refilling, this efficiency loss may be lessened or disappear altogether, as a lower value of n can significantly boost efficiency for a large aperture size (Fig. 7). Changes in n have a greater impact for larger apertures because of the relative contributions to efficiency of the contraction phase and the refill phase. A decreased n reduces the work wasted during refill, which is a greater component of efficiency when the aperture is large, but has no effect on work wasted during contraction, which is a greater component of efficiency when the aperture is small. Empirical determination of this coefficient would aid our understanding of efficiency tradeoffs in larger squid.

Our model predicts that maximal efficiency for squid jet propulsion is found at 1 cm ML. Smaller and larger squid have complex behavioral options for maximizing efficiency, which we have only begun to understand.

MATERIALS AND METHODS

Animal collection

Paralarvae of *Dosidicus gigas* (d'Orbigny 1835) were obtained from a naturally deposited egg mass collected in the Guaymas Basin of the Gulf of California, Mexico, on 21 June 2006 (Staaf et al., 2008). Filming of these paralarvae occurred 3–6 days after hatching.

Hatchlings were also obtained from *in vitro* fertilization, using gametes collected at Cordell Bank, California (38°0′N 123°28′W), on 13 November 2007. Details of artificial fertilization techniques are described by Staaf et al. (Staaf et al., 2011). Filming of these paralarvae occurred 1–10 days after hatching.

Video recording

Paralarvae were observed in still, natural seawater in either a rectangular 1 l acrylic aquarium or a thin viewing chamber (72×47×7 mm). Black backgrounds were placed behind both chambers to enhance visibility of the nearly transparent paralarvae.

Standard videos (30 frames s^{-1}) were taken with a DCR-TRV70 mini-DV camcorder (Sony, Tokyo, Japan) at 1080i (1920×1080 pixels). Selected sequences covering a range of swimming movements were captured with Adobe Premier 5.0 (Adobe Systems Incorporated, San Jose, CA, USA) and exported as frames into ImageJ (http://rsb.info.nih.gov/ij, National Institutes of Health, Bethesda, MD, USA) to analyze the dynamics of mantle contraction and speed of swimming.

For high-speed videos, individual paralarvae were placed in 50 mm diameter plastic culture dishes, in seawater of ~5 mm depth, underneath a dissecting microscope. A high-speed camera (Fastcam 512, Photron USA, Inc., San Diego, CA, USA) under computer control was mounted on the microscope and used to film, select and extract video clips. Recordings were made at 512×512 pixel resolution at either 125 or 250 frames s^{-1}, providing sufficient resolution to observe details of the fastest jets.

Eleven sequences of standard videos and 16 sequences of high-speed videos were extracted and analyzed. The standard sequences include data from at least three separate paralarvae obtained both naturally and by *in vitro* fertilization; the exact number is not known because of the difficulty of tracking individual paralarvae when several were present. The high-speed sequence data came from one paralarva, obtained by *in vitro* fertilization. Sequences were chosen based on the paralarva being in focus and, in the case of the 1 l aquarium, at least several body lengths away from the walls. The narrowness of the viewing chamber prevented assessment of the distance of the paralarva from the walls, and in the case of the Petri dishes, avoiding wall effects was not possible.

Ambient temperature during the video trials ranged from 18–20°C, comparable to the temperatures *D. gigas* paralarvae would usually experience in the wild and well within the range of optimum temperature for development (Staaf et al., 2011).

Kinematic measurements

All video clips were analyzed frame by frame with ImageJ. In each frame, we measured mantle width (MW) at the widest part of the mantle (approximately one-third of the mantle length from the head) and dorsal mantle length (ML). Mantle aperture width, the opening of the mantle just behind the head, was also measured in the high-speed videos. As the exact distance of the squid from the camera could not always be determined, especially in the 1 l aquarium, dorsal ML was used to normalize all measurements. ML is invariable because of the presence of the pen acting as a stiffener (Packard, 1969; Ward, 1972; Packard and Trueman, 1974).

Minimal MW was calculated by dividing the narrowest normalized MW in each clip by the widest MW measured in that clip. Mantle aperture width was divided by head width; a value of 1 indicates a complete seal between head and mantle and values larger than 1 indicate leakage around the head through the mantle opening.

Swimming speed was measured as the number of MLs traveled per second, based on frame rate. Contraction time was determined by counting the number of frames between the fully expanded mantle and the minimal MW and dividing by frame rate. Mantle contractions were counted in each clip, and the rate of mantle contraction, or jet frequency, was calculated as the number of mantle contractions per second.

The statistics package R (R Development Core Team, 2005) was used to create a generalized linear model (GLM) for squid velocity, using these empirical variables of contraction time, minimal mantle width and mantle aperture width. The GLM was analyzed with ANOVA to determine the relative contribution to velocity of each variable.

Modeling

A model of squid jet propulsion was built in MATLAB (MathWorks, Inc., Natick, MA, USA), using three primary hydrodynamic components – thrust, drag and effective mass (see below) – to calculate speed, mantle-cavity pressure and whole-cycle efficiency of a swimming squid. We considered only active swimming in the posterior direction (i.e. in the direction of the fins), and squid movement in this direction was considered positive.

For most model runs, the squid was assumed to be neutrally buoyant, with a density equal to that of seawater. However, to model the vertical jetting behavior of paralarvae, squid density was set to 1055 kg m^3 (O'Dor, 1988a) and gravitational force was subtracted from thrust. In this situation, sinking in the negative (anterior) direction was permitted. Consideration of gravitational effects for older squid, which swim both vertically and horizontally, would necessitate expanding our one-dimensional model into two dimensions, which was beyond the scope of this study.

Thrust, T, is defined by the change in momentum of the squid's jet and calculated from the velocity of the jet relative to the squid (u_j), the density of the expelled seawater (ρ_w), and the area of the aperture through which the jet is expelled (A). The parameter A represents the entire area through which water can flow at any given time; during contraction it is the funnel aperture, and during refilling it is the mantle opening. The parameterization of A during both phases is explained in the next section.

Angular aiming or rotation of the funnel was not considered in this model, so thrust always acts on the squid in the direction opposite to that of the jet. During contraction:

$$T = \rho_w A u_j^2 . \quad (4)$$

During refilling, water can be drawn into the aperture from a hemisphere centered around the jet, with flow ranging from axial (along the body axis of the squid) to radial. The axial component of this flow contributes to thrust, whereas the radial component does not. Lacking direct information on the flow field during refilling, we instead include a coefficient n ($0<n<1$) to account for nonaxial flow. If all flow is axial, $n=1$; if all flow is radial, $n=0$:

$$T = -n\rho_w A u_j^2 . \quad (5)$$

An additional contribution to thrust can arise from any differential between the jet pressure, P_j, and the ambient water pressure, P_0. This contribution would be calculated as the difference between the two pressures multiplied by the aperture area:

$$A\left(P_j - P_0\right). \quad (6)$$

The magnitude of this term is usually quite small (Hill and Peterson, 1992), so we have omitted it from our equations. During contraction it would contribute to thrust in the same direction as jet momentum, but during refilling it could potentially counteract jet momentum thrust. Permitting the coefficient n to go slightly outside its bounds allows us to model this effect.

Let us now consider how to calculate jet velocity. The squid's mantle is considered a prolate ellipsoid and its volume calculated from mantle length, L, and mantle radius, r. The volume of water in the mantle cavity, V_i, uses the inner mantle radius, r_i, and the volume of the entire squid plus water, V_o, uses the outer mantle radius, r_o, in the following equation:

$$V = \frac{2}{3}\pi r^2 L . \quad (7)$$

Jet velocity is calculated from aperture area and the rate of change of the volume of water (V_i) inside the squid:

$$u_j = \left(\frac{1}{A}\right)\left(\frac{dV_i}{dt}\right). \quad (8)$$

During mantle contraction, volume decreases, and dV_i/dt and u_j are both negative; the jet flows in the opposite direction of squid movement. During refilling, these parameters are positive. These equations represent a significant simplification of the jet of a real swimming squid, which because of its pulsatile nature is subject to unsteady effects, particularly the formation of vortex rings (Krueger and Gharib, 2003; Dabiri et al., 2006; Bartol et al.,

The Journal of Experimental Biology (2014) doi:10.1242/jeb.082271

2009a; Bartol et al., 2009b). Accurate modeling of these effects was deemed too difficult for the present study.

Drag, F_d, is highly dependent on Reynolds number (*Re*). For $Re \leq 1$, drag can be calculated directly from the outer mantle radius, r_o, mantle length, L, seawater dynamic viscosity, μ, and squid speed, S, relative to the stationary water (Happel and Brenner, 1965):

$$F_d = \frac{8\pi\mu S\sqrt{\left(\frac{Lr_o^2}{4} - r_o^2\right)}}{\left(b^2+1\right)\coth^{-1}\left(b\right) - b}, \quad (9)$$

where b is defined as:

$$b = \frac{1}{\sqrt{1-\left(\frac{2r_o}{L}\right)^2}}. \quad (10)$$

For $Re>1$, F_d can be calculated from the squid's speed, the outer mantle radius, and the coefficient of drag, C_d.

$$F_d = -\frac{1}{2}\rho S\,|S|\,C_d\pi r_o^2. \quad (11)$$

The C_d is itself dependent on *Re*. For $Re>1000$, C_d is dependent only on the outer mantle radius and length and an empirically calculated constant, C_f=0.004 (Hoerner, 1965):

$$C_d = 0.44\frac{2r_o}{L} + 2C_f\frac{L}{r_o} + 4C_f\sqrt{\frac{2r_o}{L}}. \quad (12)$$

For intermediate *Re* between 1 and 1000, drag is not well described by simple theory. In this range, we calculated C_d by interpolating with a cubic spline between Re=1 (back-calculating C_d from F_d from Eqn 9) and Re=1000 (from Eqn 12), and used this value in Eqn 11. Fig. 9 illustrates the calculated values of drag for three sizes of squid, covering the range from $Re<1$ to $Re>1000$.

Effective mass, M_{eff}, is the sum of the squid's mass (which is the sum of the mass of the water inside the squid and the squid itself) and the added mass of water around the squid as it is accelerated. Using ρ_w as the density of seawater and ρ_s as the density of squid tissue, and following Lamb (Lamb, 1932):

$$M_{eff} = \rho_w V_i + \rho_s\left(V_o - V_i\right) + \rho_w V_o\left(\frac{a}{2-a}\right), \quad (13)$$

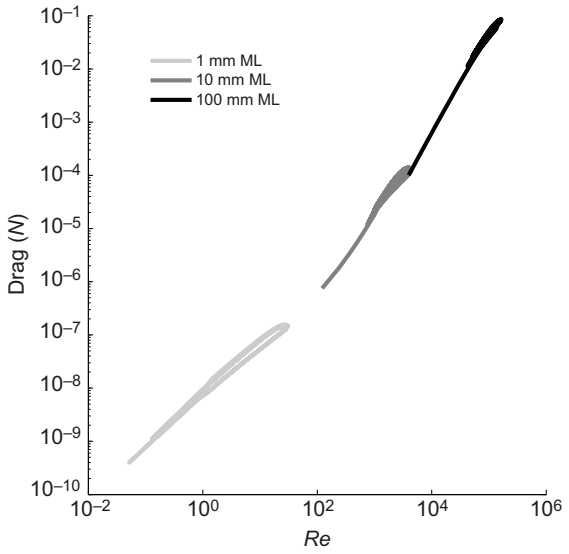

Fig. 9. Drag as a function of Reynolds number for three sizes of squid. Data for 10 cycles of contraction and refilling are plotted for each squid (1, 10 and 100 mm ML); loops emerge because drag depends on both *Re* and squid velocity.

where a is the aspect ratio of the prolate ellipsoid:

$$a = \left(\frac{1-x^2}{x^3}\right)\ln\left(\frac{1+x}{1-x} - x\right) \quad (14)$$

and x is eccentricity, calculated from outer mantle radius and length:

$$x = \sqrt{1-\left(\frac{2r_o}{L}\right)^2}. \quad (15)$$

Acceleration of the squid, dS/dt, is calculated with the standard equation for variable-mass motion:

$$\frac{dS}{dt}M_{eff} = F_d + u_j\frac{dM_{eff}}{dt}, \quad (16)$$

where the derivative of M_{eff} is approximated as:

$$\frac{dM_{eff}}{dt} \approx \rho_w\frac{dV_i}{dt}. \quad (17)$$

Using Eqns 8 and 9 we obtain:

$$\frac{dS}{dt} = \frac{F_d + T}{M_{eff}}. \quad (18)$$

We then calculate S by integrating numerically over time with a fourth-order Runge–Kutta routine (Jameson et al., 1981).

We considered mantle cavity pressure from two independent sources: direct, from the squeeze of contracting mantle muscle during thrust, and indirect, from viscous effects as water is forced through the funnel aperture. Johnson et al. (Johnson et al., 1972) related direct pressure from thrust, P_T, to thrust and aperture area with the following equation:

$$T = 2dP_T A. \quad (19)$$

The coefficient of discharge, d, was calculated by these authors to be ~0.6; however, this was for a system with a constant aperture area. O'Dor showed that a d of 1 can be used in a system in which A varies over the course of the jetting cycle. Thus we arrive at an equation for P_T (O'Dor, 1988a):

$$P_T = \frac{T}{2A}. \quad (20)$$

Indirect pressure from viscous effects (P_μ) depends on the dynamic viscosity of seawater (μ), the aperture radius (r_a), and the rate of flow. We calculate rate of flow as volume change inside the mantle (dV_i/dt). The following relationship is given by Happel and Brenner (Happel and Brenner, 1965):

$$P_\mu = -\frac{\kappa\mu\frac{dV_i}{dt}}{r_a^3}, \quad (21)$$

where κ is a constant determined by the *Re* of flow through the aperture. Happel and Brenner provide a theoretical value of 3 for *Re* approximately <3, which we used in our calculations (Happel and Brenner, 1965).

Summing the two pressure terms gives total mantle-cavity pressure, P, the relevant value from the perspective of the squid's mantle muscle:

$$P = \frac{T}{2A} - \frac{\kappa\mu\frac{dV_i}{dt}}{r_a^3}. \quad (22)$$

The pressure value can then be used to calculate stress in the mantle muscle, because the force that pressurizes water in the mantle cavity must be counteracted by an equal force in the mantle itself. Pressure acts over the longitudinal cross-sectional area of the mantle cavity: $2r_iL$ if we assume the mantle is a simple cylinder, a reasonable simplification of a prolate ellipsoid for these purposes. Stress, σ, acts over the cross-sectional area of the mantle muscle: $2Lw$, where w is the thickness of the mantle muscle (calculated from r_o and r_i as detailed in the next section). We can therefore set:

$$P\left(2r_iL\right) = \sigma\left(2Lw\right), \quad (23)$$

which can be simplified to produce an equation for stress:

$$\sigma = \frac{Pr_i}{w}. \quad (24)$$

The Journal of Experimental Biology (2014) doi:10.1242/jeb.082271

Our final calculation concerns efficiency. Anderson and DeMont showed that Froude efficiency, which assumes steady flow and an upstream intake of fluid, is inappropriate for squid jet propulsion, with its unsteady flow and downstream intake (Anderson and DeMont, 2000). Instead, we follow Anderson and Grosenbaugh in considering hydrodynamic efficiency (η) to be useful power divided by total power, where total power is useful power plus wasted power (Anderson and Grosenbaugh, 2005). Useful power is jet thrust multiplied by squid speed, and wasted power comes from the kinetic energy left in the wake by the jet that did not impart thrust to the squid.

Kinetic energy is determined from mass and velocity. The mass of fluid in the jet over a given time is determined by fluid density, aperture area and the absolute value of jet velocity:

$$\rho_w A\,|u_j|. \tag{25}$$

The velocity of this mass relative to still water is given by the difference between jet velocity and squid velocity, so wasted power from kinetic energy is:

$$\frac{1}{2}\rho_w A\,|u_j|\left(u_j+S\right)^2. \tag{26}$$

We thus arrive at an equation for efficiency:

$$\eta=\frac{TS}{TS+\frac{1}{2}\rho_w A\,|u_j|\left(u_j+S\right)^2}. \tag{27}$$

Our aim was to calculate efficiency over the entire jetting cycle, both contraction and refilling, for a squid that intends to move in a forward direction. In this context, backward movement reduces efficiency. Therefore, we used Eqn 27 when S was positive. When S was negative, we changed the numerator to zero, preventing backward motion from being considered useful. This exclusion causes our calculation to diverge from other propulsive efficiencies, such as Froude or rocket motor, that permit backward motion to contribute positively.

Note that when u_j=–S, no momentum is left in the wake, and jetting is 100% efficient. In our model, values contributing to η were summed over 10 jet cycles to integrate the change in efficiency as the squid approaches a steady-state pattern of jetting from a starting velocity of zero.

Mantle contraction and refilling were effected by linearly varying the mantle radius between a maximal value at the beginning of contraction to a minimal value at the beginning of refill. The choice of maximal and minimal values is explained in the next section.

To study the importance of aperture control, aperture radius (and therefore area) was either kept constant throughout the jetting cycle, or varied linearly, increasing to its maximum 20% of the way through the cycle (O'Dor, 1988b; Bartol et al., 2001) and then decreasing to its minimum.

Fig. 10 illustrates the model output for 10 jet cycles of a 1 mm ML squid with constant aperture radius.

Parameterization

To evaluate the scaling of jet propulsion with size, we provided the model with mantle length only. This simplified the analysis, allowing us to focus on size by maintaining consistent relationships between morphological parameters. We used the regression equations of Stevenson, which are based on a variety of squid species, to calculate mantle radius, mantle thickness and funnel radius, all of which vary allometrically with mantle length (Stevenson, 1996). Jet frequency as a function of mantle length was calculated according to a regression equation provided by R. K. O'Dor (personal communication). These regression equations are plotted in Fig. 8 (straight lines), along with measurements taken by the authors and gleaned from the literature.

The degree by which mantle radius decreases during contraction is itself somewhat size dependent, although the most commonly reported value across a range of species is a 30% reduction from fully expanded to fully contracted (Packard, 1969; Gosline and DeMont, 1985; Gosline and Shadwick, 1983; Preuss et al., 1997). For an ontogenetic series of *S. lessoniana*, Thompson and Kier measured a reduction of 40% in 5–10 mm ML, 32% in 11–25 mm ML, 31% in 26–40 mm ML and 28% in 60–100 mm ML individuals. For modeling purposes, we used cubic splines to interpolate between these values for squid in the given sizes ranges (Thompson and Kier, 2001). For squid smaller than 5 mm ML, we set the reduction to a constant 40%, and for squid larger than 100 mm ML, 28%.

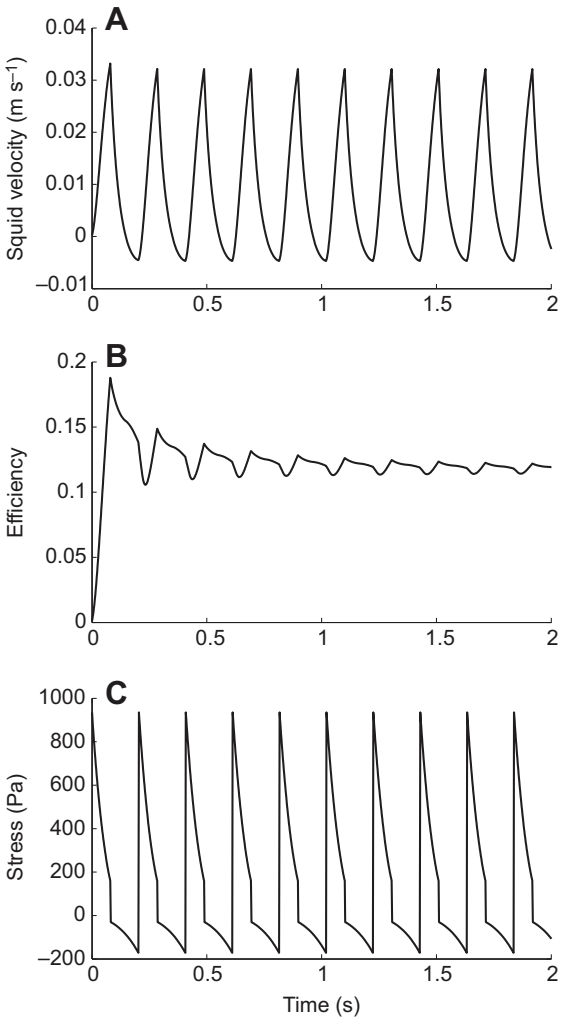

Fig. 10. Theoretical jet propulsion by a 1 mm ML squid swimming for 10 cycles of contraction and refilling. All parameters were calculated with the regression equations shown in Fig. 3. (A) Squid velocity, (B) propulsive efficiency and (C) stress in the mantle muscle.

We did not attempt to model the distinctive characteristics of escape jets, which include hyperinflation of the mantle (e.g. Thompson and Kier, 2001) and retraction of the head into the mantle aperture (e.g. Packard, 1969). These features increase the total volume of water expelled from the mantle, and escape jets therefore present both increased velocity and mantle cavity pressure compared with regular jets (Otis and Gilly, 1990).

The regression in Fig. 8B provides resting mantle thickness, w_r. As the mantle contracts, its thickness increases. Because the total volume of mantle muscle must remain constant, mantle thickness at any time t during contraction can be calculated from the following equation [derived from setting resting volume equal to contracted volume, and also independently derived by MacGillivray et al. (MacGillivray et al., 1999)]:

$$w_t = r_t - \sqrt{r_t^2 - w_r\left(2r_{max} - w_r\right)}. \tag{28}$$

For Eqn 23, we are only interested in one component of the mantle: the circular muscle fibers that act to squeeze the water inside the mantle cavity. Circular muscle makes up the majority of the mantle, about 91% of total volume. The remainder of the mantle is taken up primarily by radial muscle, with collagen fibers forming as little as 0.2% of the total mantle by weight (Gosline and Shadwick, 1983; Gosline and DeMont, 1985). Circular muscle fibers are further specialized into CMP and SMR fibers (Preuss et al., 1997).

These two fiber types may be recruited at different swimming speeds, with CMP fibers providing power for fast swimming and escape jets and SMR fibers for slow jetting (Thompson et al., 2008). For the sake of simplicity, our model considers all circular muscle together and adjusts mantle thickness accordingly by a factor of 0.91.

Similarly, Thompson et al. showed that strain – the amount of muscle deformation due to stress – varies significantly across the mantle wall, with muscles near the inner surface experiencing higher strain rates than those near the outer surface (Thompson et al., 2010b). Although this feature is no doubt important to squid, we chose to exclude it from our model, instead assuming that the forces produced and experienced by all the circular muscles fibers are equal at each time point.

Each jetting cycle consists of a period of contraction, during which the mantle radius decreases, and a period of refilling as mantle radius increases. Thompson and Kier present data for hatchling and young *S. lessoniana* showing the time spent in contraction is roughly equal to that spent in refilling, but this is not a universal feature of jetting (Thompson and Kier, 2001). Bartol et al. report a contraction period for hatchling *D. pealeii* that lasts 23% of the total jet period (Bartol et al., 2009a). Anderson and Grosenbaugh report the jet period of adult *D. pealeii* taking 31% and the refilling period 46% of each cycle, with the remaining 23% not categorized (Anderson and Grosenbaugh, 2005). O'Dor reports a total cycle length for adult *D. opalescens* of 1.5 s, with refilling beginning after 0.6 s, which would give 40% and 60% for jetting and refilling, respectively (O'Dor, 1988b). The ratio of refilling to jetting times thus appears to be dependent on both size and species of squid. We chose to use a contraction:refilling ratio of 40:60 in our model to incorporate a marginally shorter contraction period, to be consistent with the above literature.

The final parameter of concern is the size of the aperture through which the jet flows. During the contraction phase of the cycle, the mantle opening is closed by one-way valves on either side of the head, and water flows only through the funnel. Funnel aperture was calculated from funnel radius based on the regression in Fig. 8C. During the refilling phase of the jet cycle, the valves open and the funnel closes (Ward, 1972), so the relevant aperture is the mantle opening. This area is calculated as twice the open-funnel aperture (Anderson and Grosenbaugh, 2005). As no empirical data were available to parameterize the coefficient of nonaxial flow, n, it was set to 1 for model runs that explored the impact of other parameters. It was then varied between 1 and 0 to explore the full potential range in reduction of thrust due to nonaxial intake of water.

In the simplest version of the model, funnel area is held constant throughout contraction, with aperture area determined by the regression in Fig. 8C. This is considered the 'maximal funnel area'. In order to investigate the effect of dynamic control of the funnel during jetting, we added a layer of complexity whereby the funnel radius expands to reach the maximal value 20% of the way through the contraction phase of the cycle (O'Dor, 1988b; Bartol et al., 2001; Dabiri and Gharib, 2005), then decreases to 20% of this value (Bartol et al., 2001). This is referred to as 'variable funnel area'. For comparison purposes, we also ran the model with the funnel radius set to a constant 20% of the maximal value, referred to as 'minimal funnel area'.

Acknowledgements
L. Zeidberg and K. Miklasz both shared their knowledge of and enthusiasm for locomotion in numerous brainstorming sessions. I. Bartol kindly provided advice and feedback in an early stage of the project. T. Smith provided assistance with Matlab, and A. Staaf offered many physical and mathematical insights.

Competing interests
The authors declare no competing financial interests.

Author contributions
D.J.S. conceived and designed the study, collected and analyzed the empirical data, programmed the final model, and drafted and revised the article. W.F.G. helped conceive and design the study, offered guidance on data collection and analysis, and made substantive improvements to the article. M.W.D. also helped with study conception and design, data collection and analysis, made substantive improvements to the article, and wrote the original prototype of the model. All three authors worked together to interpret the findings.

Funding
This work was funded by a Graduate Research Fellowship from the National Science Foundation to D.J.S.; a Dr Nancy Foster Scholarship from the National Oceanic and Atmospheric Administration [grant number NA08NOS4290446 to D.J.S.]; the National Science Foundation [grant numbers OCE 0526640 and OCE 0850839 to W.F.G.]; and the David and Lucille Packard Foundation [grant number 2008-32708 to W.F.G.].

References
Alexander, R. M. and Goldspink, G. (1977). *Mechanics and Energetics of Animal Locomotion*. London: Chapman and Hall.
Anderson, E. J. and DeMont, M. E. (2000). The mechanics of locomotion in the squid *Loligo pealei*: locomotory function and unsteady hydrodynamics of the jet and intramantle pressure. *J. Exp. Biol.* **203**, 2851-2863.
Anderson, E. J. and Grosenbaugh, M. A. (2005). Jet flow in steadily swimming adult squid. *J. Exp. Biol.* **208**, 1125-1146.
Bartol, I. K., Patterson, M. R. and Mann, R. (2001). Swimming mechanics and behavior of the negatively buoyant shallow-water brief squid *Lolliguncula brevis*. *J. Exp. Biol.* **204**, 3655-3682.
Bartol, I. K., Krueger, P. S., Thompson, J. T. and Stewart, W. J. (2008). Swimming dynamics and propulsive efficiency of squids throughout ontogeny. *Integr. Comp. Biol.* **48**, 720-733.
Bartol, I. K., Krueger, P. S., Stewart, W. J. and Thompson, J. T. (2009a). Pulsed jet dynamics of squid hatchlings at intermediate Reynolds numbers. *J. Exp. Biol.* **212**, 1506-1518.
Bartol, I. K., Krueger, P. S., Stewart, W. J. and Thompson, J. T. (2009b). Hydrodynamics of pulsed jetting in juvenile and adult brief squid *Lolliguncula brevis*: evidence of multiple jet 'modes' and their implications for propulsive efficiency. *J. Exp. Biol.* **212**, 1889-1903.
Boletzky, S. V. (1974). The "larvae" of cephalopoda: a review. *Thalassia Jugosl.* **10**, 45-76.
Chen, D. S., Van Dykhuizen, G., Hodge, J. and Gilly, W. F. (1996). Ontogeny of copepod predation in juvenile squid (*Loligo opalescens*). *Biol. Bull.* **190**, 69-81.
Dabiri, J. O. and Gharib, M. (2005). The role of optimal vortex formation in biological fluid transport. *Proc. Biol. Sci.* **272**, 1557-1560.
Dabiri, J. O., Colin, S. P. and Costello, J. H. (2006). Fast-swimming hydromedusae exploit velar kinematics to form an optimal vortex wake. *J. Exp. Biol.* **209**, 2025-2033.
Gilly, W. F., Hopkins, B. and Mackie, G. O. (1991). Development of giant motor axons and neural control of escape responses in squid embryos and hatchlings. *Biol. Bull.* **180**, 209-220.
Gilly, W. F., Zeidberg, L. D., Booth, J. A. T., Stewart, J. S., Marshall, G., Abernathy, K. and Bell, L. E. (2012). Locomotion and behavior of Humboldt squid, *Dosidicus gigas* (d'Orbigny, 1835), in relation to natural hypoxia in the Gulf of California, Mexico. *J. Exp. Biol.* **215**, 3175-3190.
Gosline, J. M. and DeMont, M. E. (1985). Jet-propelled swimming in squids. *Sci. Am.* **252**, 96-103.
Gosline, J. M. and Shadwick, R. E. (1983). The role of elastic energy storage mechanisms in swimming: an analysis of mantle elasticity in escape jetting in the squid, *Loligo opalescens*. *Can. J. Zool.* **61**, 1421-1431.
Hanlon, R. T., Hixon, R. F., Hulet, W. H. and Yang, W. T. (1979). Rearing experiments on the California market squid *Loligo opalescens* Berry 1911. *Veliger* **21**, 428-431.
Happel, J. and Brenner, H. (1965). *Low Reynolds Number Hydrodynamics*. Upper Saddle River, NJ: Prentice Hall.
Haury, L. and Weihs, D. (1976). Energetically efficient swimming behavior of negatively buoyant zooplankton. *Limnol. Oceanogr.* **21**, 797-803.
Hill, P. G. and Peterson, C. R. (1992). *Mechanics and Thermodynamics of Propulsion*, 2nd edn. Reading, MA: Addison-Wesley.
Hoar, J. A., Sim, E., Webber, D. M. and O'Dor, R. K. (1994). The role of fins in the competition between squid and fish. In *Mechanics and Physiology of Animal Swimming* (ed. L. Maddock, Q. Bone and J. M. C. Rayner), pp. 27-33. Cambridge: Cambridge University Press.
Hoerner, S. F. (1965). *Fluid-Dynamic Drag*. Bricktown, NJ, USA: Hoerner Fluid Dynamics.
Hunt, J. C., Zeidberg, L. D., Hamner, W. M. and Robison, B. H. (2000). The behavior of *Loligo opalescens* (Mollusca: Cephalopoda) as observed by a remotely operated vehicle (ROV). *J. Mar. Biol. Assoc. U. K.* **80**, 873-883.
Jameson, A., Schmidt, W. and Turkel, E. (1981). Numerical solutions of the Euler equations by finite-volume methods using Runge-Kutta timestepping. In *AIAA Paper No. 81-1259, AIAA 24th Aerospace Sciences Meeting*. Reno, NV: AIAA.
Johnson, W., Soden, P. D. and Truman, E. R. (1972). A study in jet propulsion: an analysis of the motion of the squid, *Loligo vulgaris*. *J. Exp. Biol.* **56**, 155-165.
Krueger, P. S. and Gharib, M. (2003). The significance of vortex ring formation to the impulse and thrust of a starting jet. *Phys. Fluids* **15**, 1271-1281.
Lamb, H. (1932). *Hydrodynamics*. Cambridge: Cambridge University Press.
MacGillivray, P. S., Anderson, E. J., Wright, G. M. and Demont, M. E. (1999). Structure and mechanics of the squid mantle. *J. Exp. Biol.* **202**, 683-695.
Milligan, B., Curtin, N. and Bone, Q. (1997). Contractile properties of obliquely striated muscle from the mantle of squid (*Alloteuthis subulata*) and cuttlefish (*Sepia officinalis*). *J. Exp. Biol.* **200**, 2425-2436.
O'Dor, R. K. (1988a). The forces acting on swimming squid. *J. Exp. Biol.* **137**, 421-442.

O'Dor, R. K. (1988b). Limitations on locomotor performance in squid. *J. Appl. Physiol.* **64**, 128-134.
O'Dor, R. K. and Webber, D. M. (1986). The constraints on cephalopods: why squid aren't fish. *Can. J. Zool.* **64**, 1591-1605.
O'Dor, R. K. and Webber, D. M. (1991). Invertebrate athletes: trade-offs between transport efficiency and power density in cephalopod evolution. *J. Exp. Biol.* **160**, 93-112.
O'Dor, R. K., Balch, N., Foy, E. A. and Helm, P. L. (1986). The locomotion and energetics of hatchling squid, *Illex illecebrosus*. *Am. Malacol. Bull.* **4**, 55-60.
Otis, T. S. and Gilly, W. F. (1990). Jet-propelled escape in the squid *Loligo opalescens*: concerted control by giant and non-giant motor axon pathways. *Proc. Natl. Acad. Sci. USA*, **87**, 2911-2915.
Packard, A. (1969). Jet propulsion and the giant fibre response of *Loligo*. *Nature* **221**, 875-877.
Packard, A. and Trueman, E. R. (1974). Muscular activity of the mantle of *Sepia* and *Loligo* (Cephalopoda) during respiratory movements and jetting, and its physiological interpretation. *J. Exp. Biol.* **61**, 411-419.
Preuss, T., Lebaric, Z. N. and Gilly, W. F. (1997). Post-hatching development of circular mantle muscles in the squid *Loligo opalescens*. *Biol. Bull.* **192**, 375-387.
Schaefer, K. M., Fuller, D. W. and Block, B. A. (2007). Movements, behavior, and habitat utilization of yellowfin tuna (*Thunnus albacares*) in the northeastern Pacific Ocean, ascertained through archival tag data. *Marine Biology* **152**, 503-525.
Shea, E. K. (2005). Ontogeny of the fused tentacles in three species of ommastrephid squids (Cephalopoda, Ommastrephidae). *Invertebr. Biol.* **124**, 25-38.
Staaf, D. J., Camarillo-Coop, S., Haddock, S. H. D., Nyack, A. C., Payne, J., Salinas-Zavala, C. A., Seibel, B. A., Trueblood, L., Widmer, C. and Gilly, W. F. (2008). Natural egg mass deposition by the Humboldt squid (*Dosidicus gigas*) in the Gulf of California and characteristics of hatchlings and paralarvae. *J. Mar. Biol. Assoc. U. K.* **88**, 759-770.
Staaf, D. J., Zeidberg, L. D. and Gilly, W. F. (2011). Effects of temperature on embryonic development of the Humboldt squid *Dosidicus gigas*. *Mar. Ecol. Prog. Ser.* **441**, 165-175.
Staaf, D. J., Redfern, J., Gilly, W. F., Watson, W. and Balance, L. T. (2013). Distribution of ommastrephid paralarvae in the eastern tropical Pacific. *Fish Bull.* **111**, 78-89.
Stevenson, D. (1996). *Squid Locomotion: Size Limitations on Effective And Efficient Swimming*. Honors thesis, Stanford University, Stanford, CA, USA.
Thompson, J. T. and Kier, W. M. (2001). Ontogenetic changes in mantle kinematics during escape-jet locomotion in the oval squid, *Sepioteuthis lessoniana* Lesson, 1830. *Biol. Bull.* **201**, 154-166.
Thompson, J. T. and Kier, W. M. (2006). Ontogeny of mantle musculature and implications for jet locomotion in oval squid *Sepioteuthis lessoniana*. *J. Exp. Biol.* **209**, 433-443.
Thompson, J. T., Szczepanski, J. A. and Brody, J. (2008). Mechanical specialization of the obliquely striated circular mantle muscle fibres in loliginid squids. *J. Exp. Biol.* **211**, 1463-1474.
Thompson, J. T., Bartol, I. K., Baksi, A. E., Li, K. Y. and Krueger, P. S. (2010a). The ontogeny of muscle structure and locomotory function in the long-finned squid *Doryteuthis pealeii*. *J. Exp. Biol.* **213**, 1079-1091.
Thompson, J. T., Taylor, K. R. and Gentile, C. (2010b). Gradients of strain and strain rate in the hollow muscular organs of soft-bodied animals. *Biol. Lett.* **6**, 482-485.
Vecchione, M. (1999). Extraordinary abundance of squid paralarvae in the tropical eastern Pacific Ocean during El Niño of 1987. *Fish Bull.* **97**,1025-1030.
Ward, D. V. (1972). Locomotory function of the squid mantle. *J. Zool.* **167**, 487-499.
Webber, D. M. and O'Dor, R. K. (1986). Monitoring the metabolic rate and activity of free-swimming squid with telemetered jet pressure. *J. Exp. Biol.* **126**, 205-224.
Weihs, D. (1974). Energetic advantages of burst swimming of fish. *J. Theor. Biol.* **48**, 215-229.
Yang, W. T., Hixon, R. F., Turk, P. E., Krejci, M. E., Hulet, W. H. and Hanlon, R. T. (1986). Growth, behavior and sexual maturation of the market squid, Loligo opalescens, cultured throughout the life cycle. *Fish Bull.* **84**, 771-798.
Zeidberg, L. D. (2004). Allometry measurements from in situ video recordings can determine the size and swimming speeds of juvenile and adult squid *Loligo opalescens* (Cephalopoda: Myopsida). *J. Exp. Biol.* **207**, 4195-4203.